Conservation Laws in Cancer Modeling

Antonio Fasano, Alessandro Bertuzzi, and Carmela Sinisgalli

Abstract We review mathematical models of tumor growth based on conservation laws in the full system of cells and interstitial liquid. First we deal with tumor cords evolving in axisymmetric geometry, where cells motion is simply passive and compatible with the saturation condition. The model is characterized by the presence of free boundaries with constraints driving the free boundary conditions, which in our opinion are particularly important, especially in the presence of treatments. Then a tumor spheroid is considered in the framework of the so-called two-fluid scheme. In a multicellular spheroid, on the appearance of a fully degraded necrotic core, the analysis of mechanical stresses becomes necessary to determine the motion via momentum balance, requiring the specification of the constitutive law for the "cell fluid." We have chosen a Bingham-type law that presents considerable difficulties because of the presence of a yield stress, particularly with reference to the determination of an asymptotic configuration. Finally, we report some recent PDE-based models addressing complex processes in multicomponent tumors, more oriented to clinical practice.

Keywords Conservation laws • Cancer modeling • Tumor cords • Tumor spheroids • Multicomponent tumors

A. Fasano (✉)
Dipartimento di Matematica "U. Dini", Universita' di Firenze,
Viale Morgagni 67/A, 50134 Firenze, Italy

Istituto di Analisi dei Sistemi ed Informatica "A. Ruberti" - CNR,
Viale Manzoni 30, 00185 Roma, Italy
e-mail: fasano@math.unifi.it

A. Bertuzzi • C. Sinisgalli
Istituto di Analisi dei Sistemi ed Informatica "A. Ruberti" - CNR,
Viale Manzoni 30, 00185 Roma, Italy
e-mail: bertuzzi@iasi.cnr.it; carmela.sinisgalli@iasi.cnr.it

A. d'Onofrio, A. Gandolfi (eds.), *Mathematical Oncology 2013*,
Modeling and Simulation in Science, Engineering and Technology,
DOI 10.1007/978-1-4939-0458-7_2

1 Introduction

The literature on cancer modeling has been rapidly increasing during the present century, paralleling the remarkable intensification and diversification of the research in this field. The last International Conference in Industrial and Applied Mathematics (ICIAM 2011, Vancouver) hosted a surprisingly large number of talks on that subject, emphasizing many new and important areas of investigation, including the rather new subject of the role of cancer stem cells (see, e.g., [42]). Among the recent review papers we quote [4, 7, 25, 26, 34, 51].

A feature that has been treated differently in many growth models is the one of conservation laws, accompanying the choice of the phenomena to be included in the model, such as cell displacement mechanisms (whether totally passive or with a chemotactic or haptotactic component), drug actions, angiogenesis, and so on. One of the main issues is mass conservation, which in several instances has been disregarded with the aim of producing a treatable model. Raising a far too obvious criticism may be simply not constructive, because the target of simplifying a subject whose nature is so tremendously complicated, trying to preserve the basics of biological behavior, has often proved to be useful and has to be rather assessed on the basis of the results. Take for instance the paper [35] on the acid-mediated invasion of healthy tissue by tumor cells, where only three species are present: tumor cells, normal cells, and the H^+ ions produced by tumor cells and attacking the other species. The model does not specify how the acidity is produced (thus glucose metabolism is completely absent), it does not consider any interstitial fluid carrying nutrients, and not even oxygen consumption. Nevertheless it reproduces at least qualitatively the main biological phenomenon, emphasizing the presence of a gap between the advancing and the receding species, represented in a one-dimensional geometry by travelling waves, for appropriate values of the parameters. The richness of that oversimplified model has been further clarified in the paper [27]. A nontrivial extension has been presented very recently in [36]. In our opinion this is a remarkable example of how effective a lean model can be, provided it is constructed assembling the essential elements. Without entering the elegant and appealing subject of travelling waves in tumors, we quote the recent paper [56] in which a three-species model (tumor, normal, and dead cells) described by a treatable system of PDEs describes the spread of an aggressive glioma in the form of a diffusion-dominated spherical expanding wave.

"Completeness" remains of course a legitimate aspiration, worth to be pursued with some caution. The quotation marks allude to the extremely hard task not only of putting all the relevant ingredients but then of specifying how they mutually interact. Such an attempt necessarily calls for choices, which in most cases have some degree of arbitrariness: cell–cell and cell–matrix interactions, active or passive cell displacement, cytoskeleton and membrane mechanics, cells electrochemistry, signaling, cell metabolism (aerobic or anaerobic), proliferation, death and degradation, mutations, interstitial fluids, angiogenesis (including vessels sprouting, leaking and occlusion), metastatic processes, dormancy, etc. For each element the model formulation requires the selection of constitutive laws, containing

parameters of various nature, whose numerical value has to be provided, at least in a reasonable range. In some cases the latter task may be prohibitive. When we introduce the cell-killing action of drugs, we are faced with the problem of transport through vasculature and through the interstitial liquids, with the interaction with the cell membrane and with the various cell components. Not to speak of the mechanics of the tumor mass as a whole and its modification following treatments it is, we believe, sufficiently clear that completeness is an objective which makes sense only leaving an exceedingly complex reality and restricting the area to specific aspects. What is reasonable is trying to attain some degree of accuracy focusing on the most relevant elements in the particular process considered. For sure in this framework conservation laws are invariably the backbone of any mathematical schematization.

In this paper we want to go through the literature of the last decade or so taking conservation laws as the leading subject, trying to emphasize the diversity of various approaches, both in the modeling and in the scopes.

A striking example is the case we are going to deal with in Sect. 2, the so-called tumor cords, for which we summarize a two-fluid model keeping the mechanics at a very simple level but emphasizing some nontrivial mathematical aspects arising in the presence of massive cell death due to treatments. In our opinion this crucial feature has not received enough attention in the literature.

The other class of problems in cancer modeling with a simple geometry is the one of multicellular spheroids, which, in the framework of continuum mechanics, are treated as spheres with all quantities depending just on time and on the radial coordinate. This kind of symmetry is even more treatable than the not-so-nice axisymmetric geometry of tumor cords, since for instance all fluxes are just radial, though it does not always allow to skip the analysis of the stress field. The literature is huge and deals with many fundamental subjects. In the recent review paper [24] the important question of incorporating glucose metabolism has been discussed at length, together with the noticeable consequence of pH decrease. Therefore we will not insist here on such a question. Instead in Sect. 3 we analyze a refinement of the two-fluid scheme in which the "cell fluid" exhibits a yield stress, i.e., a Bingham fluid. This approach, first presented in [2] and further developed in [57], has been studied extensively in [15]. Occasionally we will point out some basic differences accompanying the switch from axisymmetric geometry (cords) to spherical symmetry, which for instance deeply influences the structure of the necrotic region. In both cases it turns out that the mechanical behavior of the necrotic region has a crucial influence on the evolution of the tumor, a fact that deserves to be greatly emphasized and that has been discussed in the review paper [25].

The first two sections, based on our work, are mainly concentrated on mass and momentum balance and its implications on the mechanical behavior of systems possessing an idealized geometry. The models considered there incorporate the continuous mass exchange between cells and interstitial fluid. In such a framework it is possible to analyze the role of mechanics in full detail and to carry out a complete investigation of the mathematical structure of the problem. The reader may object that, in spite of its mathematical complexity, such an approach has a rather limited target in the much wider horizon of malignancies and of their treatments. Indeed, great efforts are being made to produce mathematical models

for the growth of specific tumors and related therapies in the presence of concurrent phenomena. For this reason in the last section we report some recent researches, taken from the literature, addressing complex processes in multicomponent tumors, confining our attention to the class of models expressed through systems of partial differential equations. Though obviously not exhaustive, the choice is certainly quite representative of the positive trend to get modeling closer to clinical practice.

2 Tumor Cords and the Doubly Constrained Boundary Conditions

In the three papers [8–10] some peculiar features that may occur in cancer growth have been pointed out for the first time in the framework of the microstructures, mainly observed in experimental tumors, where tumor cells proliferating around a blood vessel form an approximately axisymmetric aggregate called tumor cord. Generally tumor cords have different sizes and orientation and may or may not be surrounded by necrosis [44, 53, 65]. Despite its complexity, the model described in [8, 9] was based on a rather naïve description of cell metabolism, since oxygen was the only "nutrient" considered. A novel feature at that time was instead the analysis of the flow of the interstitial fluid from the central vessel to the cord periphery [10]. The introduction of free boundaries, such as the sharp interface between viable and necrotic tissue, led to the formulation of boundary conditions depending on the system evolution and regulated by suitable constraints. A fundamental simplification was provided by the assumption that the cords are arranged in a regular array of parallel identical elements, so that, because of symmetry, the cords are separated by no-flux boundaries forming a bee nest structure. As a consequence, an individual cord can be studied, approximating the hexagonal boundary with a cylinder, so that the whole system is axisymmetric (Fig. 1).

Though computationally complicated, the partition of the cord (Fig. 2) by means of cylindrical interfaces separating homogeneous species has the advantage of facilitating the calculation of the cell and fluid velocity fields. In the quoted papers the analysis of well posedness was fully performed, along with the study of important qualitative properties. Concerning our principal theme, namely conservation laws, *the interstitial liquid plays the basic role of allowing the fulfillment of mass balance*. Indeed, the fluid provides the material for the production of new cells and receives the material released by the degradation of dead cells in the necrotic region. The cell-liquid mass exchange looks quite natural, but it requires the analysis of fluid motion, which is not trivial. As a matter of fact, often in the literature the shortcut is taken by simply ignoring the liquid. For example, in the early age of cancer modeling, Greenspan [38] introduced some volume loss rate after necrosis and his choice was adopted by many authors, even recently, though the actual removal mechanism has never been specified. Such a particular aspect in cancer modeling has been extensively discussed in [25] with special attention to the consequences for the attainment of a steady state. It has to be said that, however strange it

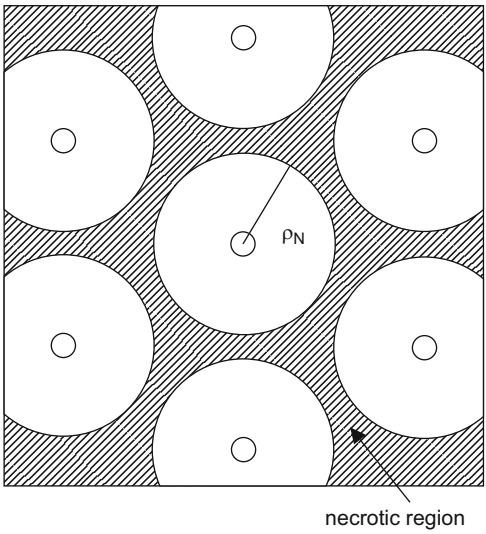

Fig. 1 Sketch of the cross section of a regular array of tumor cords exhibiting the presence of a necrotic region (at distance ρ_N from the cord axis). *Small circles* are cross sections of vessels. Each cord is surrounded by a no-flux surface, approximated by a *cylinder*

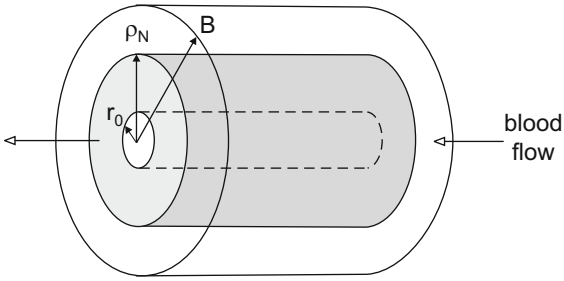

Fig. 2 Sketch of a single cord, externally bounded by the no flux surface $r = B$ and showing the viable region (in *grey*)

may look, models not including a basic element like the interstitial fluid can be meaningful if, as we said in the introduction, such a simplification is introduced in a suitable way, so as to capture anyway some essential phenomena. Moreover, in the scheme below, the cell motion is completely passive, generated by proliferation, thus disregarding the autonomous motility (haptotaxis, chemotaxis) as well as the random motility (diffusion). Nevertheless, for the case of cords, and even more for the case of multicellular spheroids that will be considered later, neglecting such causes of motion looks reasonable.

Still considering the kinematic aspect, we note that once the tumor has spread longitudinally along the vessel, the average motion of cells takes place in the radial direction. The question of tumor progression along the vessel has been considered in [5] in a different framework (cord expansion against a host tissue).

Coming back to the system sketched in Fig. 2, we treat the cell-liquid system as a mixture, adopting the scheme of continuum mechanics. Clearly, this is not the only possible choice. Discrete or hybrid models have been used extensively and with some success (see, e.g., [1, 43]). Continuum models are justified in the presence of a sufficiently large number of cells. It could be objected that for the typical cord

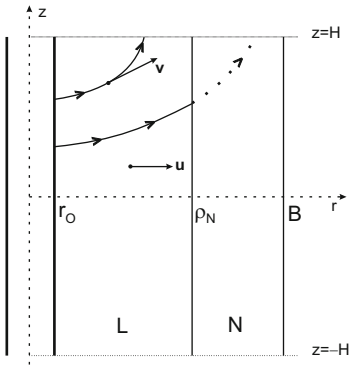

Fig. 3 Sketch of velocity fields: cellular velocity **u**; radial, fluid velocity **v**. The liquid enters the cord crossing the wall of the axial blood vessel. Viable and necrotic regions are indicated by L and N, respectively

size (a radius of the order of ten cell diameters) the latter requirement is not met. However, we must consider that a representative volume element is a cylindrical shell of radius smaller than a cell diameter, extending over the whole length of the vessel (up to 1 mm), actually intersecting a large number of cells, so that the continuum approach ultimately makes sense.

A glance to Fig. 3 clarifies why the liquid velocity field can be taken axisymmetric, but not radial, since the fluid must be allowed to leave the cord from the extreme sections ($z = \pm H$), while instead the cell velocity field (in the continuum sense) can be taken essentially radial. Figure 3 shows also the spatial coordinates. The system is symmetric with respect to the cross section $z = 0$. Living cells occupy the region L: $r_0 < r < \rho_N$, which lies between the vessel and the necrotic region N, and when developed: $\rho_N < r < B$, where B is the outer radius of the cord. Living cells can be either proliferating (volume fraction ν_P)[1] or quiescent (volume fraction ν_Q). Dead cells are actually disseminated in the cord (their volume fraction is denoted by ν_A), but the region N is exclusively necrotic. We consider three possible causes of cell death:

(i) extreme hypoxia, occurring when the oxygen concentration σ does not exceed a viability threshold σ_N,
(ii) the action of a cytotoxic drug (or radiation), taking place with a known kinetics, and
(iii) apoptosis, also regulated by some kinetics.

As a consequence the region N is normally characterized by the inequality $\sigma \leq \sigma_N$, with the exception that will be clarified later.

A basic hypothesis is that the medium is saturated, so that the volume fraction of the extracellular liquid ν_E is complementary to the total volume fraction of the

[1] Some authors adopt the extreme view point that proliferation takes place only at the tumor surface because of contact inhibition (e.g., [17]) and then migrate, driven by the surface curvature. Here we stick to the experimental observation that in the tumors we are talking about proliferation occurs in the tumor mass, whenever enough oxygen is available.

cells, $\nu = \nu_P + \nu_Q + \nu_A = 1 - \nu_E$. All the components are assumed to have the same density. Another fundamental assumption is that ν_E is constant.

One of the most difficult aspects in modeling a growing mass is the mechanical behavior. Mixture theory (see, e.g., [58]) seems a perfect tool, since we are dealing with a multicomponent system, but, independently of the constitutive law attached to each component, the presence of mass conversion processes is a substantial difficulty. Several papers have addressed this issue in various ways. One of the first papers adopting mixture theory was [19]. In the recent paper [2] a very complex analysis of the mechanics of the cellular component has been performed justifying the presence of a yield stress and therefore of a Bingham-like constitutive law.

We will return to such a question in the next section. Here we are pursuing the aim of keeping the mechanics as simple as possible. For this reason we perform some operations that ultimately will circumvent the dynamical problem almost completely, exploiting symmetry to bypass the necessity of writing down the momentum balance equations. First of all, we adopt the so-called two-fluid approach [18], assimilating the cell aggregate to a Newtonian fluid and considering the interstitial fluid as inviscid. There are several conceptual limitations in the two-fluid scheme that have been illustrated in [25], but the advantage of dealing with clearly well-defined constituents, with the possibility of making suitable assumptions on their mutual interaction, makes it extremely valuable. As we pointed out in many instances, modeling cancer growth is a compromise between accuracy and simplicity, so that the goal is to keep as much as possible of the biology, limiting at the same time the number of physical parameters involved. Of course the hypothesis attributing no viscosity to the interstitial fluid is justified by the fact that its viscosity (comparable to the one of water) is by many orders of magnitude smaller than the viscosity of the "cellular fluid." Nevertheless, the interaction with the cells is taken into account assuming that the flow relative to the cells obeys Darcy's law:

$$\nu_E(\mathbf{v} - \mathbf{u}) = -\kappa \nabla \hat{p}\,, \tag{1}$$

where κ is the hydraulic conductivity of the cell aggregate experienced by the liquid and $\hat{p}$ is the liquid pressure.

The way of bypassing a finer description of the mechanics of the system consists in averaging two quantities in the longitudinal direction, namely the radial component of the liquid velocity $v_r(r, z, t)$ and pressure $\hat{p}(r, z, t)$, thus defining

$$v(r, t) = \frac{1}{2H} \int_{-H}^{H} v_r(r, z, t)\, dz\,, \tag{2}$$

$$p(r, t) = \frac{1}{2H} \int_{-H}^{H} \hat{p}(r, z, t)\, dz\,. \tag{3}$$

The first quantity, multiplied by $2\pi rH$, provides the total radial discharge through a surface coaxial with the central vessel. The mass balance of the components in the region L is expressed by the system

$$\begin{aligned}
&\frac{\partial v_P}{\partial t} + \frac{1}{r}\frac{\partial}{\partial r}(ruv_P) = \chi v_P + \gamma v_Q - \lambda v_P - \mu_P v_P\,,\\
&\frac{\partial v_Q}{\partial t} + \frac{1}{r}\frac{\partial}{\partial r}(ruv_Q) = -\gamma v_Q + \lambda v_P - \mu_Q v_Q\,,\\
&\frac{\partial v_A}{\partial t} + \frac{1}{r}\frac{\partial}{\partial r}(ruv_A) = \mu_P v_P + \mu_Q v_Q - \mu_A v_A\,,\\
&v_E \nabla\cdot\mathbf{v} = \mu_A v_A - \chi v_P\,,
\end{aligned} \tag{4}$$

which, together with the saturation assumption, yields the global mass balance

$$\nabla\cdot[v\mathbf{u} + v_E\mathbf{v}] = 0\,. \tag{5}$$

In (4) χ is the proliferation rate, and the coefficients γ, λ are the transition rates from the class Q (quiescent cells) to P (proliferating cells) and vice versa. They are functions of the oxygen concentration σ (γ is nondecreasing and λ nonincreasing). μ_P, μ_Q are death rates in the respective classes possibly depending on the concentration of a cytotoxic drug; μ_A is the mass conversion rate of apoptotic cells (class A) to liquid, due to degradation. If we take the longitudinal average of the longitudinal component of (5), exploiting the assumption that $\mathbf{u}$ is $u(r,t)$ times the outward directed radial unit vector, we get an equation containing the difference $v_z(r,H,t) - v_z(r,-H,t)$, whose product with v_E gives the local liquid efflux rate from the cord, for which we assume that

$$v_E[v_z(r,H,t) - v_z(r,-H,t)] = 2\zeta_{out}(p(r,t) - p_\infty)\,. \tag{6}$$

In other words, the liquid loss rate is regulated by the pressure excess with respect to a far-field pressure p_∞, established by the lymphatic system. The coefficient ζ_{out} may in principle depend on r, but is taken constant for simplicity. The procedure just described leads to the equation

$$\frac{1}{r}\frac{\partial}{\partial r}(rv) = -\frac{1}{v_E}\Big(\chi v_P - \mu_A v_A + \frac{\zeta_{out}}{H}(p - p_\infty)\Big)\,. \tag{7}$$

The longitudinal average of the radial component of (5) leads finally to express the pressure in terms of the relative liquid-cell velocity:

$$p(r,t) = p_0(t) - \frac{1-\nu}{\kappa}\int_{r_0}^{r}[v(r',t) - u(r',t)]dr'\,. \tag{8}$$

An important feature of the model is the appearance of the new unknown $p_0(t)$, i.e., the pressure at the blood vessel wall. Indeed, equation (7) requires the inlet boundary condition

$$(1-\nu)v(r_0,t) = \zeta_{in}(p_b - p_0(t)), \tag{9}$$

meaning that the liquid inflow rate from the blood vessel is proportional to the pressure jump across the vessel wall.[2] The coefficient ζ_{in} is a positive constant, and p_b is the blood pressure in the specific vessel considered. It has to be said that actually blood pressure decreases along the flow, so that p_b is a function of z (averaging out time dependence, since the time scale of heart pulsation is much smaller than the scale of tumor evolution). The feasibility of taking constant both p_b and, later on, the oxygen concentration in blood σ_b along the cord has been discussed in the paper [10], concluding that for vessels shorter than a millimeter (the case of capillaries in a vascular tumor) the approximation is compatible with the many other sources of error included in the scheme. The equation governing the cell velocity field can be derived in the form of a mass balance by summing the first three equations in (4):

$$\frac{1}{r}\frac{\partial}{\partial r}(ru) = \frac{1}{\nu}(\chi v_P - \mu_A v_A)\,, \tag{10}$$

to which the boundary condition

$$u(r_0,t) = 0 \tag{11}$$

must be associated.

Concerning oxygen, because of its large diffusivity ($D_{O_2} \simeq 10^{-5}\,\mathrm{cm}^2/\mathrm{s}$) and easy penetration through cell membrane, at each time its concentration is assumed to be at the equilibrium profile satisfying the equation

$$D_{O_2}\,\Delta\sigma = f_P(\sigma)v_P + f_Q(\sigma)v_Q\,, \tag{12}$$

where the consumption rates $f_P \geq f_Q$ are of Michaelis-Menten type.

Oxygen concentration at the blood vessel wall is taken constant (see [10] for a justification):

$$\sigma(r_0,t) = \sigma_b\,. \tag{13}$$

[2] Here we neglect osmotic pressure.

The conditions for σ at the necrotic interface (when present) are far less obvious. Considering the role of the threshold σ_N, the natural conditions for $r = \rho_N$ would be

$$\sigma(\rho_N, t) = \sigma_N \tag{14}$$

$$\left.\frac{\partial \sigma}{\partial r}\right|_{r=\rho_N} = 0\,. \tag{15}$$

The second condition is a consequence of the absence of consumption in the necrotic core and it implies that the oxygen profile in the N zone is flat. However, a model accounting for treatments must be able to describe a sudden rise in oxygen concentration due to massive cell death. When such a phenomenon takes place (an increase in σ_b would have a similar effect), the necrotic interface cannot always be identified as the level set by (14), for the simple reason that if σ rises above threshold at the necrotic interface, dead cells will not return to life. In that case σ must be left free to evolve, while the necrotic interface becomes a material surface, moving with the velocity of the viable cells that stay on it:

$$u(\rho_N(t), t) = \dot{\rho}_N(t)\,. \tag{16}$$

The state described by (16) lasts as long as $\sigma(\rho_N, t)$ remains above threshold. When the threshold is recovered, the cells resume entering the necrotic region. In summary, we conclude that:

(i) the following unilateral constraints have to be satisfied at each time instant:

$$\sigma(\rho_N, t) \geq \sigma_N \tag{17}$$

$$u(\rho_N(t), t) \geq \dot{\rho}_N(t)\,; \tag{18}$$

(ii) when one constraint is satisfied in the strict sense, the other has to hold as an equality;
(iii) equation (15) always holds true.

This very peculiar structure of the boundary conditions at the necrotic interface makes the mathematics considerably difficult.

Unfortunately, when we come to modeling the necrotic region we find more complications, because we realize that the necrotic region can be "prevalently solid" or "prevalently liquid." In the first case the degrading cells are in mutual contact and can bear an external stress, while in the opposite case the task of sustaining external stress is given to the liquid. Thus we have two regimes that we call N-solid and N-liquid, respectively. The basic time-dependent quantities to be considered, besides the interface $r = \rho_N(t)$, are

- The cord outer boundary $r = B(t)$
- The volume occupied by the degrading cell $V_N^c(t)$

- The volume occupied by the liquid $V_N^l(t)$
- The liquid pressure $p_N(t)$

The total volume $V_N(t)$ of the necrotic region is

$$V_N(t) = V_N^c(t) + V_N^l(t) = 2\pi H(B^2 - \rho_N^2)\,. \tag{19}$$

The two partial volumes evolve according to the equations

$$\dot{V}_N^c = 4H\pi\rho_N(1-\nu_E)[u(\rho_N,t) - \dot{\rho}_N] - \mu_N V_N^c\,, \tag{20}$$

$$\dot{V}_N^l = 4H\pi\rho_N\nu_E[v(\rho_N,t) - \dot{\rho}_N] + \mu_N V_N^c - q_{out}(t)\,. \tag{21}$$

In (20) the first term on the RHS is the contribution of cells entering the necrotic region (always nonnegative, as we know); the second term is the rate of conversion into liquid. In the second equation the only term to be explained is the last one:

$$q_{out} = \frac{\zeta_{out}^N}{H} V_N^l(p_N - p_\infty)\,, \tag{22}$$

namely the liquid efflux rate from the cord ends $z = \pm H$, where ζ_{out}^N is a positive coefficient.

The solid volume fraction is subject to the constraint

$$\frac{V_N^c}{V_N} \le \nu_N < 1\,, \tag{23}$$

(for the sake of generality ν_N is distinguished from ν, but in practice they can be taken equal). Now, in the N-solid regime, the above constraint is at work, so we can take

$$V_N^c = \nu_N V_N \quad \Leftrightarrow \quad V_N^l = (1-\nu_N)V_N\,, \tag{24}$$

where $V_N(t)$ has the expression (19). Thus (20) yields a differential equation for the difference $B^2 - \rho_N^2$:

$$\frac{d}{dt}(B^2 - \rho_N^2) = 2\frac{1-\nu_E}{\nu_N}\rho_N[u(\rho_N,t) - \dot{\rho}_N] - \mu_N(B^2 - \rho_N^2)\,, \tag{25}$$

and operating with (21) it is possible to express q_{out} in terms of geometrical and kinematical unknowns, which in turn allows to derive $p_N(t)$.

Let us now discuss the question of how to detect the transition to the N-liquid regime and vice versa. The key point is to monitor the pressure $p_N(t)$, comparing it with the pressure exerted on the cord by the surroundings, i.e., by the neighboring cords. Such an external pressure is due to the reaction of the host tissue to the expansion of the cord cohort and therefore is ultimately related with the size of

the individual cords, that is, with their equivalent radius B. We denote it by $\Psi(B)$, a continuous increasing function. Clearly, the N-solid regime is characterized by the fact that this pressure is fully sustained by the solid component, while $p_N(t) < \Psi(B(t))$. Therefore the N-liquid regime sets in when

$$p_N(t) = \Psi(B(t))\,, \tag{26}$$

which replaces (24), no longer valid as an equality but as the inequality $V_N^c < \nu_N V_N$. When (26) is enforced, $V_N^c(t)$ evolves according to (20) from which it can be deduced as a functional of $\rho_N(t)$ and of $u(t)$.

In conclusion, we are back to a doubly constrained problem:

$$V_N^c \le \nu_N V_N\,, \quad p_N \le \Psi(B)\,, \tag{27}$$

with at least one of the two constraint being active.

We remark that the fact that the boundary conditions are actually selected by the constraints, which come into play depending on the evolution of the system, has deep consequences on the mathematical structure. In particular, one has to be aware that not necessarily the various types of boundary conditions alternate over finite time intervals, since it cannot be excluded a priori that there are accumulation points of switching times. This circumstance requires the adoption of particular techniques in the existence proof (see the reference papers [9, 10]). It is really surprising that even at the level of a model including just some minimal requirements and with substantial simplifications, the corresponding mathematical structure is necessarily quite complicated. It seems to us that the presence of the constraints here emphasized is a major feature of the model. The fact that they actually come into play is unquestionably put in evidence by numerical simulations, as illustrated by Fig. 4 taken from [26], which shows an example of the time evolution of the cord in case of a drug affecting mainly the proliferating cells. Panel A illustrates the evolution induced by the treatment of the viable cell population, showing the ratio between the total volume per unit cord length of viable cells (P+Q) and its value at $t = 0$. The decrement of the amount of viable cells reduces oxygen consumption and thus causes a transient increase of the mean oxygen concentration (panel B). The re-oxygenation of the cord produces a recruitment of quiescent cells into proliferation. Thereafter, the populations P and Q tend to the stationary value (panel A). The radius ρ_N shows an initial shrinkage [52] followed by a regrowth (panel C). The interface ρ_N quickly becomes a material boundary, so satisfying (16), and remains material until, at about $t\chi = 3$, it becomes nonmaterial again, an event marked by a slope discontinuity. In the same panel, the time course of the boundary B is plotted. Panel D shows the time evolution of the pressure p_N and of the cellular fraction in the necrotic region. In the initial state the constraint (23) is satisfied with the equality sign and $p_N < \Psi(B)$. Due to the increased influx of liquid caused by cell death, p_N increases reaching $\Psi(B)$ at $t\chi \simeq 0.5$. At this point the regime changes, with $p_N = \Psi(B)$, and the cellular fraction goes below ν_N. During the cord regrowth, the

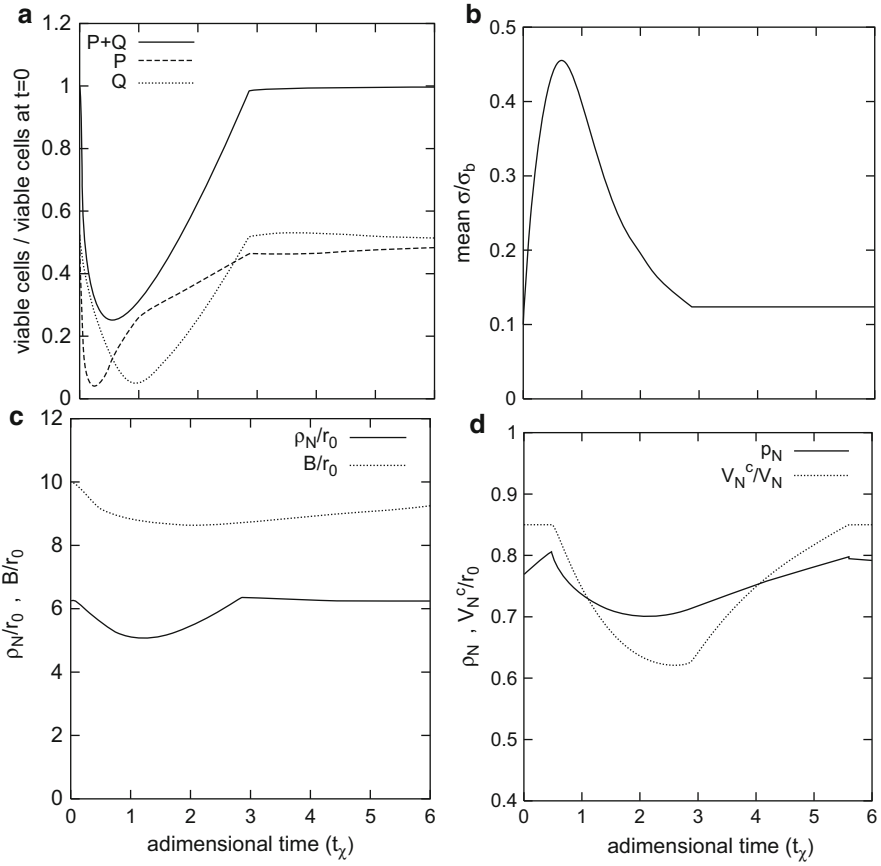

Fig. 4 *Panel A*: time course of the viable cell subpopulations after a single-dose treatment; P proliferating cells, Q quiescent cells. *Panel B*: mean oxygen concentration. *Panel C*: cord radius ρ_N and outer boundary B. *Panel D*: pressure and cell fraction in the necrotic region. Parameters values given in [26]

influx of liquid decreases and the system switches again to the regime characterized by a cellular fraction equal to ν_N ($t\chi \simeq 5.5$).

We conclude this short review about the tumor cords recalling that besides the existence and uniqueness theorem and some qualitative analysis for the doubly constrained free boundary problem, much more has been done in the wake of the papers [9, 10]. A specific analysis of interstitial pressure has been performed in [12]. One of the main aspects to be kept into account in modeling treatments is the re-oxygenation of the tumor following massive cells destruction [8]. The effects of delayed exit from quiescence after re-oxygenation were considered in [11]. The consequence of re-oxygenation on chemo- and radiotherapy has been investigated in [13,14], including the analysis of the possible advantages of dose splitting, a subject

treated in the literature in the context of the optimal fractionation of radiation dose [16, 66]. For the more general context of the application of optimization in cancer treatment, see, e.g., [49].

3 What Kind of a Fluid Can the "Cell Fluid" Be? A Model for Bingham-Like Spheroids

We have mentioned the advantages of the two-fluid approach, which, despite all the internal contradictions, have been responsible for its success. It is quite evident that the choice of identifying cells with a Newtonian fluid, which is frequent in this context, is arbitrary. In such a fluid the shear stress is generated by viscosity, whose physical origin in the case of cells should be a kind of mutual "friction." However, cells do not just slide one upon the other. Their mutual adherence is due to bonds that can resist some traction and that, when destroyed, can be restored in a different configuration. Such a situation is much more similar to what happens in "fluids" possessing some fragile internal structure, breakable by a stress beyond a threshold. This is precisely the main characteristic of Bingham fluids. Cell-exerted tractions have been measured [55] and can be surprisingly strong. Therefore it seems that resistance to motion comes primarily from the necessity of overcoming mutual bonds and then from the membrane-to-membrane friction. Accordingly, we may associate to these phenomena a nonnegligible yield stress and a viscosity, namely the two quantities intervening in the constitutive law of a Bingham fluid. The problem of finding possible steady states for a spheroid with an inner liquid core originated by dead cells degradation has been addressed in [29, 30], both in the Newtonian and in the Bingham framework, imposing the continuity of the normal stress throughout the system. Fasano et al. [29] follows a previous attempt [28] to solve the same problem imposing energy balance, stemming from the approximation that proliferating cells produce a known amount of mechanical power.

The passage from Newtonian to Bingham is by no means trivial. It is well known that defining a Bingham fluid is relatively easy in 1-D cartesian flows, but it offers different options in higher dimensions. In [15] the difficulty of selecting a constitutive law compatible with the radial motion to be found in spheroids has been emphasized, showing for instance that the definition proposed in [6] leads to a contradiction, which would make impossible to describe the early stage of the spheroid evolution. It was found in [15] that the following way of defining the stress tensor of the cell component of the mixture suites our purposes. The cellular Cauchy stress tensor in the viable region is given by

$$\mathbf{T_C} = -\nu \left(p_C + \frac{2}{3}\eta_C \nabla \cdot \mathbf{u} \right) \mathbf{I} + \nu \boldsymbol{\tau} \,, \tag{28}$$

where ν is the cell volume fraction, p_C is the cell pressure, η_C is the so-called Bingham viscosity, and $\boldsymbol{\tau}$ is the deviatoric stress tensor defined as

$$\boldsymbol{\tau} = \left(2\eta_C + \frac{\tau_0}{\sqrt{II_D}}\right)\mathbf{D} \tag{29}$$

in which, as usual, $\mathbf{D}$ is the strain rate tensor and its second invariant II_D is given in the form

$$II_D = \frac{1}{2}\mathrm{Tr}\mathbf{D}^2\,, \tag{30}$$

provided II_τ exceeds the threshold τ_0. In the opposite case we have $\mathbf{D} = 0$. We refer to [15] for additional comments on the definition (28).

The definition above applies to an aggregate of cells whose membrane is integer. We will return to the case of degrading cells later on.

The task of describing the liquid is much simpler. We put (inviscid fluid)

$$\mathbf{T}_E = \nu_E\big[-p_E\mathbf{I}\big] \tag{31}$$

with $\nu_E = 1 - \nu$, and we adopt Darcy's law for its motion relative to the cells:

$$\nu_E(\mathbf{v} - \mathbf{u}) = -\kappa\nabla p_E \tag{32}$$

thus treating the cells aggregate as a porous medium.

Remark 1. It is important that p_C and p_E be kept distinct. As a matter of fact, at the surface of the spheroid there may be forces acting differently on the two components. For instance the so-called tumor surface tension, attributable to stretched intercellular bonds, and the resistance of an external medium, like the polymer network in a gel hosting the spheroid, are applied to cells only. The concept that p_C and p_E are separate quantities has received some attention in the literature. For instance, in [48] the inequality $p_C > p_E$ was taken as a condition for cells viability.

Living cells can be proliferating or quiescent. Instead of introducing transition rates from one class to another, in [15] the two species have been separated by a sharp interface. Of course this is an extreme schematization, but, in our opinion, it does not make much difference, also owing to the uncertainty about the definition of the transition rates. The separation of a proliferating region P and a quiescent region Q, possibly surrounding a necrotic core, is very helpful to simplify the computation of the velocity field.

Again, the structure of the necrotic core N is going to play a basic role in the evolution of the system. Introducing a deterministic degradation time after which a dead cell is turned into a material mechanically behaving like a liquid, the core N is in turn divided into a liquid (NL) and a solid (NS) region. Despite the fact that

this approach is rather extreme, it finds some support in experimental observations, based on NMR techniques, pointing out a prevalence of free water in the spheroid core [54], suggesting that the NS→NL transition is due to membrane degradation.

Still under the assumption that the two components have the same density and that ν is constant, the mass balance in the various regions is expressed by the system

$$\begin{aligned}
&\nabla \cdot \mathbf{u} = \chi, && \text{in } P,\\
&\nabla \cdot \mathbf{u} = 0, && \text{in } Q \cup NS,\\
&\nabla \cdot \mathbf{v} = -\chi \frac{\nu}{1-\nu}, && \text{in } P,\\
&\nabla \cdot \mathbf{v} = 0, && \text{in } Q \cup NS \cup NL
\end{aligned} \tag{33}$$

where χ is the cell proliferation rate. The supposed constancy of ν eventually provides global mass conservation in the form of a relationship between the two radial velocity fields:

$$\nu \mathbf{u} + \nu_E \mathbf{v} = 0\,. \tag{34}$$

The fact that inertia is absolutely negligible and the analysis of the liquid-cell interaction forces lead to express the momentum balance equation for the cell component in the form

$$\nabla \cdot \mathbf{T_C} = \frac{\nu_E}{\kappa}\mathbf{u} = -\nabla \cdot \mathbf{T_E}\,. \tag{35}$$

Recalling (28), the discontinuity of $\nabla \cdot \mathbf{u}$ across the P/Q interface creates a singularity in (35), which however is easily overcome imposing the *continuity of the normal stress throughout the system*. As a matter of fact, this is one of the main assumptions in the model.

The unknown interfaces

- $r = \rho_P(t)$ between the regions P and Q
- $r = \rho_N(t)$ between the regions Q and N

are defined implicitly via the system

$$\begin{aligned}
&D_{O_2}\Delta\sigma(r,t) = f(\sigma(r,t))\nu, && \text{in P},\\
&D_{O_2}\Delta\sigma(r,t) = \frac{1}{m} f(\sigma(r,t))\nu, && \text{in Q},\\
&\sigma(R,t) = \sigma^*,\\
&\sigma(\rho_P,t) = \sigma_P,\\
&[\sigma_r(\rho_P,t)] = 0,
\end{aligned}$$

$$\sigma(\rho_N, t) = \sigma_N \,,$$
$$\sigma_r(\rho_N, t) = 0 \,, \tag{36}$$

e.g., with the choice

$$f(\sigma)\nu = nM \frac{\sigma}{H + \sigma} \,,$$

(n cell number density, M maximum consumption rate per cell, H Michaelis constant, $m > 1$, $\sigma^* > \sigma_P > \sigma_N$). It can be proved that, for a given R sufficiently large, problem (36) is uniquely solvable. Actually the qualitative nature of the solution depends on the spheroid size. The fully developed structure with the two interfaces $\rho_P(t)$, $\rho_N(t)$ is observable only for R exceeding some increasing function $R_N(\sigma^*)$, with $\sigma \equiv \sigma_N$ throughout the region N. For R below this threshold and greater than another increasing function $R_P(\sigma^*)$ there is no necrotic core and the last two conditions in (36) must be replaced with $\sigma_r(0, t) = 0$. The latter condition is still operating if $R < R_P(\sigma^*)$, in which case only the region P is present.

Unlike the previous section, here we just consider Cauchy-type boundary data on the necrotic interface, since we are only interested in the tumor growth towards its possible steady state, with no cell death cause other than hypoxia. Thus, the switch to a freely evolving oxygen concentration on the moving necrotic interface never occurs. The necrotic core will appear at the time the spheroid radius reaches the value $R_N(\sigma^*)$. The structure of the necrotic region, though not simple because of the ongoing degradation, is less complicated than in cords, for which there are constraints to be satisfied. As we said, in the approach of [15] a deterministic degradation time is introduced. Once the necrotic (hypoxic) region is formed, it keeps being fed by cells arriving from the region Q. If the necrotic core is old enough transition to "liquid" will take place, and dead cells are pushed inwards, while degrading. Of course the assumption of a fixed degradation time is artificial, not differently from all other thresholds that have been introduced. All phenomena going on in the spheroid are characterized by some degree of stochasticity; therefore all interfaces are just mathematical tools, approximating transition regions by means of sharp surfaces. Therefore a question arises very naturally: why bother with unreal pictures? The question does not apply just to the specific case at hand, but it involves the whole domain of cancer modeling, since this particular branch of biomathematics (like many others) inevitably goes through strongly simplifying assumptions and compromises. A model with no interfaces would not necessarily be more accurate, since it would anyway contain some gross approximation. Interfaces simplify the computation of the velocity fields, and this largely compensates for the mathematical complications connected to the presence of free boundaries.

If θ_D is the degradation time and t_N is the (unknown) appearance time of the necrotic core, the liquid necrotic region NL will appear at time $t_D = t_N + \theta_D$. From that time on, the NL/NS interface $r = \rho_D(t)$ will be present. Its evolution depends on the feeding rate of the region NS, which is of course one of the unknowns.

Before we move to illustrating the spheroid evolution, we have to deal briefly with the boundary conditions on the outer moving surface $r = R(t)$.

The liquid pressure equals some given external pressure (typically atmospheric pressure):

$$p_E(R,t) = p_{ext} \tag{37}$$

irrespective of whether the spheroid is grown in a water suspension or in a gel.

The computation of the cellular normal stress leads to the following equation, expressing that a jump of normal stress across the boundary is produced by surface tension. The resulting boundary condition is the following:

$$p_C(R,t) = -\frac{2}{3}\eta_C \chi + \left(2\eta_C + \frac{\tau_0}{\sqrt{II_D(R,t)}}\right) u'(R,t) + p_{ext} + \psi(R) + \frac{2\gamma}{R}\,. \tag{38}$$

where $\frac{2\gamma}{R}$ is the pressure exerted by surface tension, $\psi(R)$ is the one produced by the reaction of the host medium (gel) to the spheroid expansion, and the symbol u' is an abbreviation of $\frac{\partial u}{\partial r}$.

It has to be stressed that, even if the steady state is reached, the velocity gradient u' will not vanish at the outer surface, according to the first equation in (33). The function $\psi(R)$ is assumed to be nonnegative and Lipschitz continuous. Since it is originated by the gel deformation, namely by the displacement of the gel polymer network, it is expected to increase up to a certain value and then to stabilize.

A spheroid growing from an initial size so small that it consists entirely of the region P, evolves through the following stages:

- Stage I: fully proliferating. It ends at the time t_P at which R attains the value $R_P(\sigma^*)$.
- Stage II: the interface $r = \rho_P(t)$ appears, enclosing a quiescent core. It ends at the time t_N.
- Stage III: the region NS appears, with the boundary $r = \rho_N(t)$, but conversion to liquid is not achieved yet. It ends at time t_D.
- Stage IV: the interface $r = \rho_D(t)$ is present.

We report the main results concerning the four stages, addressing the reader to [15] for their derivation, which is definitely long and not simple. Useful pieces of information when performing the calculations are:

(i) $\nabla \cdot \mathbf{u}$ constant $\Rightarrow$ $\nabla \cdot \mathbf{D} = 0$ (however, care is needed when crossing the discontinuity of $\nabla \cdot \mathbf{u}$);

(ii) where $\nabla \cdot \mathbf{D} = 0$ the only nonzero component of the vector $\nabla \cdot \left[\left(2\eta_C + \frac{\tau_0}{\sqrt{II_D}}\right)\mathbf{D}\right]$ is the radial one, which takes the form $\frac{\tau_0}{\sqrt{II_D}}\left(-\frac{1}{2II_D}\frac{\partial II_D}{\partial r}\right)\frac{\partial u}{\partial r}$.

3.1 Stage I

All quantities can be computed explicitly:

$$u(r,t) = \frac{\chi}{3} r\,, \tag{39}$$

implying that the ODE providing the outer radius is readily solvable, leading to

$$R(t) = R_0 \exp\big(\frac{\chi}{3} t\big)\,,$$

from which we get

$$t_P = \frac{3}{\chi} \ln\big(\frac{R_P}{R_0}\big)\,.$$

Since

$$\mathbf{D} = \frac{\chi}{3}\mathbf{I}\,, \qquad II_D = \frac{\chi^2}{6}\,,$$

$$\nabla \cdot \boldsymbol{\tau} = \nabla \cdot \mathbf{D} = \mathbf{0}\,,$$

the integration of (35) with conditions (38) and (37) yields

$$p_C(r,t) = \tau_0 \sqrt{\frac{2}{3}} + p_{ext} + \psi(R) + \frac{2\gamma}{R} + \frac{\chi \nu_E}{6\nu\kappa}(R^2 - r^2) \tag{40}$$

$$p_E(r,t) = p_{ext} - \frac{\chi}{6\kappa}(R^2 - r^2)\,. \tag{41}$$

3.2 Stage II

Now we have to distinguish region P from region Q, which at this stage is an immobile core. In region P we have

$$u(r,t) = \frac{\chi}{3} r\big[1 - \big(\frac{\rho_P(t)}{r}\big)^3\big]\,, \tag{42}$$

where ρ_P is a functional of R and $R(t)$ is found by integrating the equation

$$\dot{R}(t) = \frac{\chi}{3} R(t)\big[1 - \big(\frac{\rho_P(t)}{R(t)}\big)^3\big]\,.$$

Equation (35) now gives

$$-p_C' + \tau_0 u' \Big(\frac{1}{\sqrt{II_D}}\Big)' - \frac{\nu_E}{\nu\kappa} u = 0$$

with

$$II_D = \frac{\chi^2}{3}\Big[\frac{1}{2} + \Big(\frac{\rho_P}{r}\Big)^6\Big],$$

whose integration yields

$$p_C(r,t) = p_C(R,t) - \frac{\tau_0}{\sqrt{3}}\Big\{\frac{\sqrt{2}\big[1+2\big(\frac{\rho_P}{s}\big)^3\big]}{\big[1+2\big(\frac{\rho_P}{s}\big)^6\big]^{1/2}}\Big|_r^R - 2\ln\Big[\Big(\frac{\rho_P}{s}\Big)^3 + \Big[\frac{1}{2} + \Big(\frac{\rho_P}{s}\Big)^6\Big]^{1/2}\Big]\Big|_r^R\Big\}$$
$$+\frac{\chi\nu_E}{3\nu\kappa}\Big[\frac{R^2-r^2}{2} + \rho_P^3\Big(\frac{1}{R} - \frac{1}{r}\Big)\Big], \tag{43}$$

where

$$p_C(R,t) = \frac{4}{3}\eta_C\chi\left(\frac{\rho_P}{R}\right)^3 + \tau_0\sqrt{\frac{2}{3}}\frac{1+2\left(\frac{\rho_P}{R}\right)^3}{\left[1+2\left(\frac{\rho_P}{R}\right)^6\right]^{1/2}} + p_{ext} + \psi(R) + \frac{2\gamma}{R}\,. \tag{44}$$

In the region Q, owing to the absence of motion, p_C turns out to be uniform. The discontinuity of the proliferation rate, i.e., of $\nabla\cdot\mathbf{u}$, through the P/Q interface produces a jump of p_C which can be computed imposing the continuity of the normal stress:

$$p_C(\rho_P^+,t) - p_C(\rho_P^-,t) = \frac{4}{3}\eta_C\chi + \sqrt{2}\tau_0\,. \tag{45}$$

No discontinuity is experienced by p_E which is found to be

$$p_E(r,t) = \begin{cases} p_{ext} - \dfrac{\chi}{3\kappa}(R-r)\Big(\dfrac{R+r}{2} - \dfrac{\rho_P^3}{rR}\Big), & \rho_P \le r \le R, \\ p_E(\rho_P,t), & 0 < r < \rho_P\,. \end{cases} \tag{46}$$

3.3 Stage III

The necrotic region is now present without "liquid" core. From the dynamical point of view the situation is very similar to the previous stage, the only difference being the presence of the necrotic interface $r = \rho_N(t)$, a known functional of R.

3.4 Stage IV

Stage IV evolves for $t > t_D$. As it frequently happens in tumor modeling, the structure of the necrotic region has a decisive influence on the system evolution. Here too, when entering the stage in which the liquid necrotic region appears, the mathematical nature of the problem is deeply affected. The point is that, while the liquid core is immobile, cells in its vicinity are moving inwards and we no longer have information on their velocity at the interface, while in Stage III we knew that the velocity was zero in N∪Q, hence also at $r = \rho_P(t)$. This fact introduces a very substantial complication. We emphasize the fact that the need of studying the whole stress field is originated by the necessity of determining precisely that unknown velocity.

It was therefore natural in [15] to introduce a new unknown $\omega_N(t)$ in the physical range $\omega_N(t) \leq 0$, namely the velocity of the cells crossing the interface $r = \rho_N(t)$, so that the quantity $4\pi\rho_N^2 \nu(\dot{\rho}_N - \omega_N)$ represents the feeding rate of the necrotic region. At the beginning of Stage IV $\omega_N(t_D) = 0$.

Since for $\rho_D < r < \rho_P$ the cell velocity field in that region is divergence free, we have

$$u(r,t) = \frac{1}{r^2}\rho_N^2(t)\omega_N(t)\,, \qquad \rho_D \leq r \leq \rho_P\,, \tag{47}$$

and

$$u(r,t) = \frac{1}{r^2}\rho_N^2(t)\omega_N(t) + \frac{\chi}{3}\Big(r - \frac{\rho_P^3(t)}{r^2}\Big)\,, \qquad \rho_P \leq r \leq R\,. \tag{48}$$

From the latter we deduce the differential equation for $R(t)$, namely

$$R^2(t)\dot{R}(t) = \rho_N^2(t)\omega_N(t) + \frac{\chi}{3}(R^3(t) - \rho_P^3(t))\,. \tag{49}$$

Of course the equation contains the new unknown $\omega_N(t)$. Following the motion of a dead cell through the region NS during the degradation time θ_D, we find that $\rho_D(t)$ is expressed in terms of $\omega_N(t)$ as follows:

$$\frac{1}{3}[\rho_D^3(t) - \rho_N^3(t-\theta_D)] = \int_{t-\theta_D}^{t} \rho_N^2(\tau)\omega_N(\tau)\,d\tau\,. \tag{50}$$

At this point it is clear that the determination of the kinematic unknown $\omega_N(t)$ relies on the stress analysis. In order to proceed further, we have to say something more on the degradation process, which affects the dynamical behavior. In [15] it was assumed that *membrane degradation is accompanied by a reduction of the yield stress*. This requires monitoring the age from death, $\theta(r,t)$, of cells located at a given

point of NS. Proceeding as in the derivation of (50), the latter quantity is found to have the implicit expression

$$\frac{1}{3}\big[r^3-\rho_N^3(t-\theta(r,t))\big]=\int_{t-\theta(r,t)}^{t}\rho_N^2(\tau)\omega_N(\tau)\,d\tau\,. \tag{51}$$

Now the yield stress varies in NS according to the formula

$$\tilde{\tau}_0(r,t)=\begin{cases}\tau_0, & \rho_N\le r\le R,\\ \tau_0\big[1-\frac{\theta(r,t)}{\theta_\tau}\big]_+, & \rho_D<r<\rho_N,\end{cases} \tag{52}$$

i.e., it reduces linearly to zero in the time θ_τ, which is between 0 and θ_D. This generates a new free boundary $r=\rho_\tau(t)$, tending to ρ_N or to ρ_D in the respective limits $\theta_\tau\to 0$ or $\theta_\tau\to\theta_D$. In any case, the yield stress is gone when the interface ρ_D is reached. Once more, the choice was to introduce a deterministic law, extrapolating from the biological randomness of the phenomenon in agreement with the general deterministic setting of the entire model.

The new condition at our disposal, which closes the model, is the continuity of the normal stress across the interface ρ_D. Concerning p_E, we know that it is continuous everywhere, while the just-mentioned condition of normal stress continuity eventually yields the following limit for p_C when approaching ρ_D from the "solid" side:

$$p_C(\rho_D^+,t)-2\eta_C u'(\rho_D^+,t)=p_E(\rho_D,t)\,. \tag{53}$$

In view of Remark 1 about the comparison between the two pressures p_C, p_E, the following result from [15] is of some interest: $\omega_N<0\Rightarrow p_C>p_E$, stressing the physical relevance of the orientation of the cell motion at the necrotic interface.

We just report the full expression of (53) in the case $\theta_\tau\to 0$, which requires a special procedure, referring to [15] for the more general case:

$$\begin{aligned}\frac{2\gamma}{R}=&-\psi(R)+4\eta_C\rho_N^2\omega_N\Big(\frac{1}{R^3}-\frac{1}{\rho_D^3}\Big)+\frac{4}{3}\eta_C\chi\Big[1-\Big(\frac{\rho_P}{R}\Big)^3\Big]\\&-\frac{1}{\nu\kappa}\Big\{\rho_N^2\omega_N\Big(\frac{1}{\rho_D}-\frac{1}{R}\Big)+\frac{\chi}{3}(R-\rho_P)^2\Big(\frac{1}{2}+\frac{\rho_P}{R}\Big)\Big\}\\&+\frac{2}{\sqrt{3}}\tau_0\ln\frac{\Big(\frac{\rho_P}{\rho_N}\Big)^3\Big[1+\sqrt{\frac{\chi^2\rho_P^6}{6\big(\frac{\chi}{\sqrt{3}}\rho_P^3-\sqrt{3}\rho_N^2\omega_N\big)^2}+1}\Big]}{\Big(\frac{\rho_P}{R}\Big)^3+\sqrt{\frac{\chi^2\rho_P^6}{6\big(\frac{\chi}{\sqrt{3}}\rho_P^3-\sqrt{3}\rho_N^2\omega_N\big)^2}+\Big(\frac{\rho_P}{R}\Big)^6}}\,.\end{aligned} \tag{54}$$

In (54), the fractions having ρ_D in the denominator are potentially singular at the beginning of Stage IV. The presence of the term ω_N/ρ_D^3, which cannot be balanced by any other term, says in particular that, when $t \to t_D^+$, $\omega_N(t)$ is infinitesimal (as predicted) of the same order as ρ_D^3. Moreover, owing to the sign restriction over ω_N, the limit of the ratio above has to be nonpositive. This requires a condition that, for convenience, in [15], has been imposed in the strict sense. Again we write it only with reference to the special case $\theta_\tau \to 0$, namely

$$\frac{2\gamma}{R} + \psi(R) - \frac{4}{3}\eta_C \chi\Big[1 - \Big(\frac{\rho_P}{R}\Big)^3\Big] + \frac{1}{\nu\kappa}\frac{\chi}{3}(R-\rho_P)^2\Big(\frac{1}{2} + \frac{\rho_P}{R}\Big) - \frac{2}{\sqrt{3}}\tau_0 \ln\left[\Big(\frac{\rho_P}{\rho_N}\Big)^3 \frac{1+\sqrt{\frac{3}{2}}}{\Big(\frac{\rho_P}{R}\Big)^3 + \sqrt{\frac{1}{2} + \Big(\frac{\rho_P}{R}\Big)^6}}\right] > 0\,. \tag{55}$$

This inequality is actually a limitation on the choice of the two quantities γ and τ_0, but a biological explanation is missing.

Another assumption is made on the function f expressing the oxygen absorption rate in (36) that we write in the form

$$f(\sigma) = \tilde{f}(\sigma) + (m-1)\tilde{f}(\sigma_P)H(\sigma - \sigma_P)\,, \tag{56}$$

where H is the Heaviside function and $\tilde{f}(\sigma)$ is a continuously differentiable function of Michaelis-Menten type. It is required that for all $R > R_D$,

$$R^2\Big[\frac{1}{6} - \frac{1}{2}\Big(\frac{\rho_N}{R}\Big)^2 + \frac{1}{3}\Big(\frac{\rho_N}{R}\Big)^3\Big] \sup_{\sigma\in(\sigma_N,\sigma^*)} |\tilde{f}'| < 1\,, \tag{57}$$

which makes sense because the quantity $R^2\Big[\frac{1}{6} - \frac{1}{2}\Big(\frac{\rho_N}{R}\Big)^2 + \frac{1}{3}\Big(\frac{\rho_N}{R}\Big)^3\Big]$ is bounded for $R > R_D$. In addition, $(m-1)\tilde{f}(\sigma_P)$ is supposed to be sufficiently small (for the details see [15]).

The stated conditions on ψ, f, together with (55), have been employed in [15] to show existence and uniqueness for Stage IV, first in a neighborhood of t_D and then extended by means of a standard argument.

The proof is very long and it goes through the study of how σ and the interfaces ρ_P, ρ_N depend on R. More precisely a priori estimates of the derivatives $\frac{\partial\sigma}{\partial R}$, $\frac{\partial\rho_P}{\partial R}$, $\frac{\partial\rho_N}{\partial R}$ have been obtained in terms of the data, which are instrumental in the fixed point argument employed in the proof.

Besides the well-posedness analysis, in [15] numerical simulations have been performed, dealing with the nontrivial question of selecting appropriate values for the parameters and investigating the possible attainment of a steady state. The problem is characterized by a rather large uncertainty about some critical parameters in the model, a constant obstacle in this kind of research. The tumor hydraulic

conductivity κ appearing in Darcy's law (32) is certainly one of such parameters. A chosen value was $\kappa = 4 \cdot 10^{-8}\,\mathrm{cm^3{\cdot}s/g}$ (or alternatively $4 \cdot 10^{-9}\,\mathrm{cm^3{\cdot}s/g}$), much larger than the values usually reported for solid tumors in consideration of the relatively low value of the cell volume fraction ($\nu \sim 0.6$) in spheroids. Concerning the rheological parameters of the Bingham-like cell fluid, the value $\eta_C = 10^4\,\mathrm{g/(cm{\cdot}s)}$ is acceptable, in view of the results of [45]. The determination of the yield stress τ_0 can be deduced on the basis of the measurements of the force F able to detach two adhering cells [55], according to the formula $\tau_0 = Fn^{2/3}$. The so-called tumor surface tension γ is apparently related to the upper bound of adhesion forces, hence to τ_0, as it was already observed in [29].

The interplay between τ_0 and γ is crucial for the existence of a steady state. This fact emerges very clearly when looking for the spheroid size at a possible steady state. The investigation of the possible equilibrium can be performed with the help of equation (54), in which ω_N has to be replaced with

$$\omega_N = -\frac{\chi}{3\rho_N^2}\left(R^3 - \rho_P^3\right) \tag{58}$$

which is the cell velocity at the necrotic interface corresponding to a steady spheroid of radius R. Indeed, for a spheroid at the steady state the cell velocity vanishes at the outer surface, providing the information that allows the computation of the whole velocity profile. The radius ρ_D of the inner liquid core and the age from death $\theta(r)$ can be found in terms of R:

$$\rho_D^3 = \rho_N^3 - \chi\theta_D(R^3 - \rho_P^3)\,, \tag{59}$$

$$\theta(r) = \frac{\rho_N^3 - r^3}{\chi(R^3 - \rho_P^3)}\,, \qquad \rho_D \le r \le \rho_N\,. \tag{60}$$

Thus all elements are available to formulate the steady-state version of normal stress continuity condition, which, still in the limit $\theta_\tau \to 0$, turns out to be

$$\begin{aligned} 2\gamma + R\psi(R) = {} & \frac{4}{3}\eta_C\,\chi R\frac{R^3 - \rho_P^3}{\rho_D^3} + \frac{\chi R^3}{3\nu\kappa}\left\{\frac{R}{\rho_D}\left[1 - \left(\frac{\rho_P}{R}\right)^3\right] - \frac{3}{2}\left[1 - \left(\frac{\rho_P}{R}\right)^2\right]\right\} \\ & + \frac{2}{\sqrt{3}}\tau_0 R\ln\left(\frac{\rho_P}{\rho_N}\right)^3 \frac{\left(\frac{R}{\rho_P}\right)^3 + \sqrt{\frac{1}{2} + \left(\frac{R}{\rho_P}\right)^6}}{1 + \sqrt{\frac{3}{2}}}\,, \end{aligned} \tag{61}$$

where ρ_D is expressed by (59) and ρ_P, ρ_N are known functionals of R.

The above formula allows to establish the conditions ensuring the existence of a steady state. For instance, in the case $\psi = 0$, the plot in Fig. 5 compares the

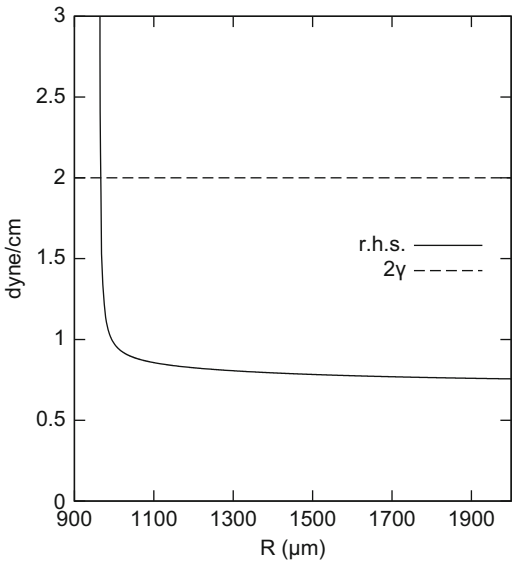

Fig. 5 Profile of right-hand-side (*solid*) and left-hand-side (*dashed*) of (61) as a function of R. $\gamma = 1\,\text{dyne/cm}$, $\tau_0 = 10\,\text{dyne/cm}^2$. Other parameters given in [15]. The predicted stationary radius is $R = 966\,\mu\text{m}$

LHS 2γ with the RHS in a case exhibiting an intersection. From (61) it is clear that for a solution to exist it is necessary that γ is large enough. Of course a mechanical reaction from the environment, meaning $\psi > 0$, helps in reaching the equilibrium. Since the RHS of (61) can be shown to go to infinity as $R \to \infty$, the equation can have two roots. The physical one is the smaller, since it is reached as an asymptotic state. The larger one is normally too big and it looks nonphysical.

The whole evolution model has been numerically simulated in [15] with the same data as in Fig. 5. The results are shown in Fig. 6, in which the moving boundaries entering the problem are followed from their origin to their asymptotic value (upper panel) and the velocity ω_N (appearing simultaneously with the interface ρ_D) is shown to reach the final value (58).

As we said, equation (61) may have no solution at all, meaning that the spheroid grows to infinity. Such a possibility has been numerically investigated too, but the values to be attributed to γ and τ_0 were out of the expected physical range.

It is legitimate to ask whether a tumor spheroid reaching equilibrium is actually observable. In principle the answer is positive, and it has to be said that experimental measurements (see, e.g., [33]) may suggest that this is indeed the case. However, it is impossible from a few experimental points to infer more than a trend to reach equilibrium, and experiments performed over a very long time show that spheroids may go into a state of senescence [31] no longer describable with a model for a viable system.

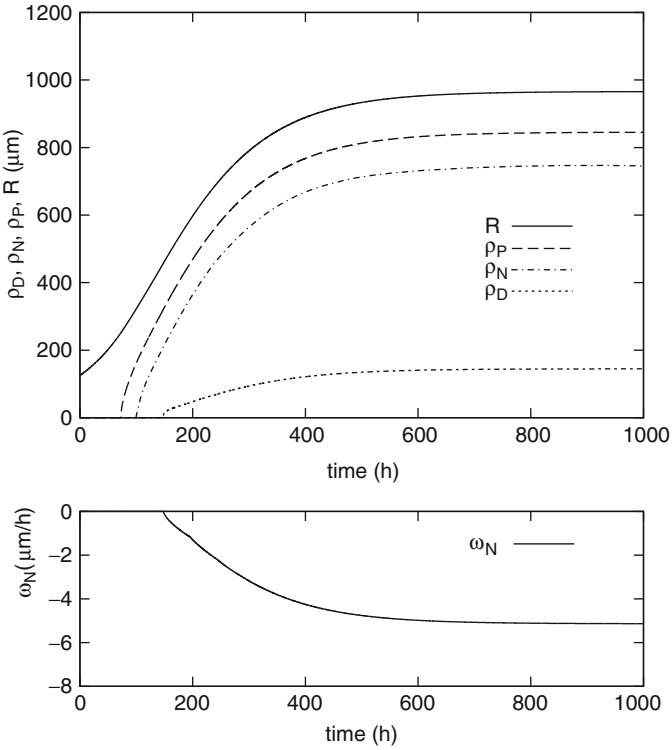

Fig. 6 *Upper panel*: Time evolution of the external radius and of all the interfaces. The velocity ω_N is reported in the *lower panel*. $\gamma = 1\,\text{dyne/cm}$, $\tau_0 = 10\,\text{dyne/cm}^2$. Other parameters given in [15]

4 Recent Models for Multicomponent Systems

In this final section, we review some very recent cancer growth models taken from the literature that include more elements than just a species of tumor cells. Active cell displacement (chemotaxis and haptotaxis) along with diffusion transport is considered, e.g., in the context of angiogenesis. Chemotaxis and reaction-diffusion are very large subjects entering those kinds of models. For them we refer to the important review papers [40,41], without mentioning their general features. Here we are more concerned in highlighting the efforts in cancer modeling to tackle problems having an immediate clinical impact. We confine our attention to models describing the spatial structure of the tumor and utilizing partial differential equations. Among compartmental models we quote for instance the paper [47], dealing with the treatment of prostate cancer by means of the so-called androgen ablation therapy, which is a very good example of how to keep the level of complexity within manageable limits, still retaining the essential pieces of information, and reaching conclusions of theoretical and practical interest. We summarize here just two models

concerning systems with many cellular and molecular species. We remark that a common trend is to ignore the contribution of interstitial fluids to the mass balance and that in both instances the model setting is such to avoid the analysis of stresses. In this sense the present section is complementary to the previous ones.

4.1 Gliomas Invasion and Angiogenesis: Diffusion Driven Processes

Since the discovery of the tumor angiogenic factor (TAF) [32] (see [59] for the historical aspects), the phenomenon of angiogenesis has been investigated for long time in two main directions: modeling its development [3, 20, 50] and modeling the action of antiangiogenic drugs [22, 39, 62]. Recently a new subject emerged, related to the chaotic structure of tumor vascularization, partly immature and leaking and with numerous loops, slowing down blood circulation in vascularized tumors and consequently reducing the efficiency of drugs delivery within the tumor mass. In [37, 46] the so-called pruning procedure was illustrated, consisting in a partial destruction of the vasculature preceding drug administration (see also [22]), so to facilitate the tumor perfusion. Here we have no space to deal with the huge topics of angiogenesis, and we concentrate on one very specific theme: the recent claim that high-grade gliomas receive their aggressiveness from angiogenesis. The reference paper is [64] (see also the literature quoted therein), which is in the wake of an earlier model proposed in [63] where diffusion was assumed to be an important (though slow) transport mechanism for cells. In the model of [64] the tumor cells can be in two states (normoxic and hypoxic), depending on the vasculature density, considered to be the direct oxygen source. Only normoxic cells proliferate. Death rates are different for the two species. The vasculature development is driven by VEGF (vascular endothelial growth factor), produced by living tumor cells. The unknowns are:

- c, normoxic cells concentration
- h, hypoxic cells concentration
- n, necrotic cells concentration
- v, vascular endothelial cells concentration
- a, VEGF concentration

Moreover, the following fractions have some role:

- $V = v/(c+h+v)$ (endothelial cells vs. the total oxygen consuming population)
- $T = (c + h + v + n)/k$ (total number of cells compared to the carrying capacity k).

The model is summarized as follows (we do not comment on the meaning of the parameters):

$$\frac{\partial c}{\partial t} = \nabla \cdot [D(1-T)\nabla c] + \rho c(1-T) + \gamma hV - \beta c(1-V) - \alpha_n nc, \tag{62}$$

$$\frac{\partial h}{\partial t} = \nabla \cdot [D(1-T)\nabla h] - \gamma hV + \beta c(1-V) - \alpha_n nh - \alpha_h h(1-V), \tag{63}$$

$$\frac{\partial n}{\partial t} = \alpha_h h(1-V) + \alpha_n n(c+h+v), \tag{64}$$

$$\frac{\partial v}{\partial t} = \nabla \cdot [D_v(1-T)\nabla v] + \mu \frac{a}{K_m + a} v(1-T) + \gamma hV - \alpha_n nv, \tag{65}$$

$$\frac{\partial a}{\partial t} = \nabla \cdot (D_a \nabla a) + \delta_c c + \delta_h h - q \frac{a}{K_m + a} v(1-T) - \omega av - \lambda a\,. \tag{66}$$

Thus cell diffusion is limited by a crowding effect, expressed by the factor $(1-T)$, which also limits proliferation of normoxic cells and of endothelial cells; the factors V and $(1-V)$ control the $c \leftrightarrow h$ transitions, and all the rest needs no explanations. The model does not consider extracellular matrix and the consequent occurrence of haptotaxis nor the chemotactic motion of endothelial cells.

The paper [64] contains an interesting discussion about the combined influence on growth of angiogenesis, diffusivity, proliferation rate, and transitions $h \to c$ and $c \to h$. The interesting conclusion is that increased aggressiveness is not necessarily originated by mutations affecting D and ρ. Even if the invasion rate is known to be strictly related to the parameters D and ρ, the final outcome is strongly conditioned by the tumor ability of developing a vascularization.

As a final remark to this subsection, we stress the fact that cell motility is a subject that has been approached in many different ways in the literature. For instance, in connection with the role of diffusivity in cancer invasion, it is worth mentioning the paper [43], preceding [64], which adopts a similar scheme in a larger context, since, besides the equations for the three species of tumor cells, and the equations for endothelial cells and for VEGF, it includes the equation for oxygen diffusion-consumption and for the development of the extracellular matrix (inducing haptotaxis of normoxic tumor cells). In that paper cell motility is treated in a very different way, since hypoxic and apoptotic cells are considered immobile and normoxic cells have a diffusivity made of two terms: a background random diffusivity D, like in (62), and an additional term, which, with the same symbols used above, is expressed by $D_c \max[c - c^*, 0]$, where c^* is some threshold concentration. The meaning of this extra term is a "pressure-driven" motility due to crowding, thus representing an opposite point of view with respect to (62), where crowding was opposing diffusion. More specifically, both D and D_c are taken to be of the same order $10^{-9}\,\mathrm{cm}^2\cdot\mathrm{s}^{-1}$. Moreover, in [43] the equation governing vascularization includes the usual chemotactic term, differently from the simpler process described by (65).

4.2 The Anti-angiogenic Role of Macrophages During Cancer Growth

We are now back to angiogenesis, but in a different perspective. In the paper [21] a mathematical model has been developed accounting for an important action of tumor-associated macrophages (TAMs). In hypoxic conditions such cells are chemically induced by tumor cells to produce VEGF, precisely as tumor cells do. However, when treated with another growth factor, namely GM-CSF (granulocyte/macrophage colony stimulating factor), TAMs are strongly stimulated to produce the VEGF inhibitor sVEGFR-1, namely the soluble VEGF receptor-1, which neutralizes VEGF by binding to it [23]. The paper [21] is based on the experimental work illustrated in [60, 61] about the influence of the transcription factors HIF-1α, HIF-2α on the production of VEGF and sVEGFR-1, respectively, studied by comparing the tumor development in normal mice and in mice with genetically induced deficiency of either factors. Interestingly enough, in view of the discussion in the previous subsection, cells diffusivity is totally disregarded, as it is very small in most tumors (here we are dealing with breast cancer). For the reader's convenience we try to preserve, as long as possible, the symbols already adopted in the previous section. Differently from that approach, the model of [21] does not deal with normoxic and hypoxic tumor cells as different species.

Thus, from the list of the previous section we remove the unknown h. Now c represents the concentration of living tumor cells with no further specification, and to the symbol list we add:

- m, macrophages concentration
- p, q, g, concentrations of specific cytokines (to be explained soon)
- s, sVEGFR-1 concentration
- w, oxygen concentration

The cytokines entering the model are:

- MCP-1/CCL2 (monocyte chemoattractant protein-1: p), produced by TAMs in response to M-CSF (q), acts as a chemoattractant to recruit more macrophages
- M-CSF (macrophage colony stimulating factor: q), produced by tumor cells, stimulates the secretion of MCP-1/CCL2 by TAMs
- GM-CSF (g), already mentioned

The transcription factors HIF-1α, HIF-2α intervene by regulating the production rates of VEGF, sVEGF-1 (without a kinetics of their own).

Let us write down the governing differential system, according to [21], which includes also the tumor velocity field $\boldsymbol{\upsilon}$:

$$\frac{\partial c}{\partial t} + \nabla \cdot (c\,\boldsymbol{\upsilon}) = \lambda_1(w)c(1 - \frac{c}{k}) - \lambda_2(w)c - \mu_c c, \tag{67}$$

where $\lambda_1(w)$ (proliferation rate) is a piecewise linear, increasing function connecting zero (for low w) to the value λ_1, through two thresholds $w_h < w_0$, and $\lambda_2(w)$ (hypoxia-induced necrosis) is a piecewise linear, decreasing function connecting the value λ_2 (for low w) to zero across two thresholds $w_n < w_h$. Then we have

$$\frac{\partial n}{\partial t} + \nabla \cdot (n\,\boldsymbol{v}) = \lambda_2(w)c + \mu_c c - \mu_n \frac{w}{w_0} m n, \tag{68}$$

where the last term describes clearance by macrophages. Equations (67) and (68) are to be solved in the unknown domain $\Omega(t)$ occupied by the tumor and embedded in a larger domain D, in which the complement to $\Omega(t)$ is occupied by the host tissue. Thus the problem contains the free boundary $\partial\Omega(t)$. Moreover,

$$\frac{\partial m}{\partial t} + \nabla \cdot (m\,\boldsymbol{v}) = -\nabla \cdot (k_p m \nabla p) - \nabla \cdot (k_g m \nabla g), \tag{69}$$

expressing mass balance of macrophages under the two chemotactic motions induced by p and g, to be solved in the whole domain D, as well as all the remaining equations for the molecular components p, q, a, s, g. The mass balance equation for the last cellular species is the one for endothelial cells:

$$\frac{\partial v}{\partial t} + \nabla \cdot (v\,\boldsymbol{v}) = -\nabla \cdot (k_a v \nabla a)\,. \tag{70}$$

Next we write the mass balance equations for the cytokines, VEGF and its inhibitor, and the drug.

$$\frac{\partial p}{\partial t} + \nabla \cdot (p\,\boldsymbol{v}) = \nabla \cdot (D_p \nabla p) + \lambda_4(w) \frac{q}{q + q_0} m - \mu_p p \tag{71}$$

with $\lambda_4(w)$ a stepwise increasing function with values $(0,\ 0.4\lambda_4,\ \lambda_4)$ through the same thresholds as $\lambda_2(w)$,

$$\frac{\partial q}{\partial t} + \nabla \cdot (q\,\boldsymbol{v}) = \nabla \cdot (D_q \nabla q) + \lambda_3 c - \mu_q q \tag{72}$$

$$\frac{\partial a}{\partial t} + \nabla \cdot (a\,\boldsymbol{v}) = \nabla \cdot (D_a \nabla a) + \lambda_5(w)c + \theta_1 \lambda_6(w) \frac{q}{q + q_0} m - \bar{\mu}_s s a - \mu_a a \tag{73}$$

where both $\lambda_5(w)$ and $\lambda_6(w)$ are proportional to another piecewise linear function $\phi(w)$ increasing from 0 to 0.3 through three thresholds $w_n < w^* < w_0$. We remark

the appearance of the coefficient θ_1, linked to the level of the transcription factor HIF-1α (set equal to 1 for normal level). For the sVEGFR-1 and the oxygen we have:

$$\frac{\partial s}{\partial t} + \nabla \cdot (s\,\boldsymbol{v}) = \nabla \cdot (D_s \nabla s) + \theta_2 \lambda_7 \frac{g + \beta g_0}{g + g_0} m - \bar{\mu}_a a s - \mu_s s \tag{74}$$

$$\frac{\partial w}{\partial t} + \nabla \cdot (w\,\boldsymbol{v}) = \nabla \cdot (D_w \nabla w) + \lambda_8 v - \lambda_9 m w - \lambda_{10} c w \tag{75}$$

where the coefficient θ_2 in (74) has for HIF-2α a role parallel to the one of θ_1 for HIF-1α and the term $\lambda_8 v$ in (75) represents oxygen delivery by endothelial cells.

The mass balance equation introducing the treatment by GM-CSF is

$$\frac{\partial g}{\partial t} + \nabla \cdot (g\,\boldsymbol{v}) = \nabla \cdot (D_g \nabla g) + f(t) - \mu_g g \tag{76}$$

with $f(t)$ expressing the drug injection rate.

All transport terms contain the velocity field $\boldsymbol{v}$ and, as we have seen in several instances, its determination is a quite delicate issue, since in general it calls for the investigation of the whole mechanics of the system (constitutive equations, momentum balance, etc.). As in the case of Sect. 2, imposing saturation and dealing with a simple geometry reduces that complex dynamical problem to a much simpler kinematical condition, since transport velocity is ultimately forced by the ideal arrangement imposed to the set of volume occupying components. Thus, if one considers just a spherical geometry, with the tumor occupying a sphere $r < R(t)$, the velocity being purely radial, and takes the sum $c + n + m + v$ constant, the equation for the only scalar component of $\boldsymbol{v}$ is derived summing up the equations for all cells mass balance. Then imposing that the boundary $r = R(t)$ moves with the cell velocity provides the necessary free boundary condition. After a long discussion on the selection of the parameters, numerical simulations show the consistency of the model with the experimental results of [60, 61].

5 Conclusions

We have reviewed a few mathematical models of tumor growth based on conservation laws and pursuing different targets. In Sects. 2 and 3 we consider tumors with only two components: cells and extracellular fluid, taking advantage of the small number of constituents to carry out the analysis of mass and momentum balance, as well as of the mathematics involved to a full extent.

The model in Sect. 2 deals with tumor cords evolving in axisymmetric geometry, where the cells motion is simply passive and compatible with the saturation condition. The main difficulty there consists in the presence of free boundaries with constraints driving the free boundary conditions, with severe mathematical and

numerical implications which in our opinion are particularly important. Though those results are not extremely recent, we decided to include them anyway in our review in order to reaffirm the crucial role of constraints, particularly in the presence of treatments. All the other material here exposed is taken from quite recent publications.

In Sect. 3 a tumor spheroid is considered in the framework of the so-called two-fluid scheme. In a multicellular spheroid, unlike the previous case, on the appearance of a fully degraded necrotic core the analysis of mechanical stresses becomes necessary to determine the motion via momentum balance, requiring the specification of the constitutive law for the cell "liquid." The case in which such a liquid is of Bingham type presents considerable difficulties linked to the presence of the yield stress that have been described, particularly with reference to the determination of an asymptotic configuration.

Despite the formidable mathematical complexity of the models treated in Sects. 2 and 3, the fact remains that two-component tumors are in a sense too schematic structures. Therefore, in the last section we illustrated two very recent studies dealing with multicomponent tumors, in order to give at least a feeling of the trends in the mathematical modeling of complex tumor structures, based on conservation laws, though in a perspective rather different from the one pursued in the models of Sects. 2 and 3. The specific studies considered are (i) Gliomas invasion and angiogenesis (reference paper [64]) and (ii) the anti-angiogenic role of macrophages during cancer growth (reference paper [21]). These are extremely interesting cases both for the modeling technique and under the perspective of their practical implications.

We regret that, because of space limitations, we could only illustrate a limited number of models. A typical feature of this research field is that it is expanding at an impressive rate, and as mathematicians come closer to the clinical practice their models become oriented to more specific targets. Despite its conciseness, we hope that our exposition can be stimulating.

References

1. T. Alarcón, H.M. Byrne, P.K. Maini, A cellular automaton model for tumour growth in inhomogeneous environment. J. Theor. Biol. **225**, 257–274 (2003)
2. D. Ambrosi, L. Preziosi, Cell adhesion mechanisms and stress relaxation in the mechanics of tumours. Biomech. Model. MechanoBiol. **8**, 397–413 (2009)
3. A.R.A. Anderson, M.A.J. Chaplain, Continuous and discrete mathematical models of tumor-induced angiogenesis. Bull. Math. Biol. **60**, 857–999 (1998)
4. R.P. Araujo, D.L.S. McElwain, A history of the study of solid tumour growth: the contribution of mathematical modelling. Bull. Math. Biol. **66**, 1039–1091 (2004)
5. S. Astanin, A. Tosin, Mathematical model of tumour cord growth along the source of nutrient. Math. Model. Nat. Phenom. **2**, 153–177 (2007)
6. I.V. Basov, V.V. Shelukhin, Generalized solutions to the equations of compressible Bingham flows. Z. Angew. Math. Mech. **79**, 185–192 (1999)

7. N. Bellomo, N.K. Li, P.K. Maini, On the foundations of cancer modelling: selected topics, speculations, and perspectives. Math. Mod. Meth. Appl. Sci. **18**, 593–646 (2008)
8. A. Bertuzzi, A. d'Onofrio, A. Fasano, A. Gandolfi, Regression and regrowth of tumour cords following single-dose anticancer treatment. Bull. Math. Biol. **65**, 903–931 (2003)
9. A. Bertuzzi, A. Fasano, A. Gandolfi, A free boundary problem with unilateral constraints describing the evolution of a tumour cord under the influence of cell killing agents. SIAM J. Math. Anal. **36**, 882–915 (2004)
10. A. Bertuzzi, A. Fasano, A. Gandolfi, A mathematical model for tumor cords incorporating the flow of interstitial fluid. Math. Mod. Meth. Appl. Sci. **15**, 1735–1777 (2005)
11. A. Bertuzzi, A. Fasano, L. Filidoro, A. Gandolfi, C. Sinisgalli, Dynamics of tumour cords following changes in oxygen availability: a model including a delayed exit from quiescence. Math. Comput. Model. **41**, 1119–1135 (2005)
12. A. Bertuzzi, A. Fasano, A. Gandolfi, C. Sinisgalli, Interstitial pressure and extracellular fluid motion in tumour cords. Math. Biosci. Eng. **2**, 445–460 (2005)
13. A. Bertuzzi, A. Fasano, A. Gandolfi, C. Sinisgalli, Cell resensitization after delivery of a cycle-specific anticancer drug and effect of dose splitting: learning from tumour cords. J. Theor. Biol. **244**, 388–399 (2007)
14. A. Bertuzzi, A. Fasano, A. Gandolfi, C. Sinisgalli, Reoxygenation and split-dose response to radiation in a tumour model with Krogh-type vascular geometry. Bull. Math. Biol. **70**, 992–1012 (2008)
15. A. Bertuzzi, A. Fasano, A. Gandolfi, C. Sinisgalli, Modelling the evolution of a tumoural multicellular spheroid as a two-fluid Bingham-like system. Math. Mod. Meth. Appl. Sci. **23**, 2561–2602 (2013)
16. A. Bertuzzi, C. Bruni, F. Papa, C. Sinisgalli, Optimal solution for a cancer radiotherapy problem. J. Math. Biol. **66**, 311–349 (2013)
17. A. Brú, S. Albertos, J.L. Subiza, J. López García-Asenjo, I. Brú, The universal dynamics of tumor growth. Biophys. J. **85**, 2948–2961 (2003)
18. H.M. Byrne, J.R. King, D.L.S. McElwain, L. Preziosi, A two-phase model of solid tumour growth. Appl. Math. Lett. **16**, 567–573 (2003)
19. H.M. Byrne, L. Preziosi, Modelling solid tumour growth using the theory of mixtures. Math. Med. Biol. **20**, 341–366 (2003)
20. M.A. Chaplain, S.R. McDougall, A.R. Anderson, Mathematical modeling of tumor-induced angiogenesis. Annu. Rev. Biomed. Eng. **8**, 233–257 (2006)
21. D. Chen, J.M. Roda, C.B. Marsh, T.D. Eubank, A. Friedman, Hypoxia inducible factors-mediated inhibition of cancer by GM-CSF: a mathematical model. Bull. Math. Biol. **74**, 2752–2777 (2012)
22. A. d'Onofrio, A. Gandolfi, Chemotherapy of vascularised tumours: role of vessel density and the effect of vascular "pruning". J. Theor. Biol. **264**, 253–265 (2010)
23. T. Eubank, R.D. Roberts, M. Khan, J. Curry, G.J. Nuovo, P. Kuppusamyl, C. Marsh, Granulocyte macrophage Colony-Stimulating factor inhibits breast cancer growth and metastasis by invoking an anti-angiogenic program in tumor-educated macrophages. Cancer Res. **69**, 2133–2140 (2009)
24. A. Fasano, Glucose metabolism in multicellular spheroids, ATP production and effects of acidity, in *New Challenges for Cancer Systems Biomedicine*, ed. by A. d'Onofrio, Z. Agur, P. Cerrai, A. Gandolfi (Springer, to appear)
25. A. Fasano, A. Gandolfi, The steady state of multicellular tumour spheroids: a modelling challenge, in *Mathematical Methods and Models in Biomedicine*, ed. by U. Ledzewicz, H. Schaettler, A. Friedman, E. Kashdan (Springer, New York, 2012), pp. 161–179
26. A. Fasano, A. Bertuzzi, A. Gandolfi, Mathematical modelling of tumour growth and treatment. In: *Complex Systems in Biomedicine*, ed. by A. Quarteroni, L. Formaggia, A. Veneziani (Springer, Italia, Milano, 2006), pp. 71–108
27. A. Fasano, M.A. Herrero, M. Rocha Rodrigo, Slow and fast invasion waves in a model of acid-mediated tumour growth. Math. Biosci. **220**, 45–56 (2009)

28. A. Fasano, M. Gabrielli, A. Gandolfi, The energy balance in stationary multicellular spheroids. Far East J. Math. Sci. **39**, 105–128 (2010)
29. A. Fasano, M. Gabrielli, A. Gandolfi, Investigating the steady state of multicellular spheroids by revisiting the two-fluid model. Math. Biosci. Eng. **8**, 239–252 (2011)
30. A. Fasano, M. Gabrielli, A. Gandolfi, Erratum to: investigating the steady state of multicellular spheroids by revisiting the two-fluid model. Math. Biosci. Eng. **9**, 697 (2012)
31. J. Folkman, M. Hochberg, Cell-regulation of growth in three dimensions. J. Exp. Med. **138**, 745–753 (1973)
32. J. Folkman, E. Merler, C. Abernathy, G. Williams, Isolation of a tumor fraction responsible for angiogenesis. J. Exp. Med. **133**, 275–288 (1971)
33. J.P. Freyer, R.M. Sutherland, Regulation of growth saturation and development of necrosis in EMT6/Ro multicellular spheroids by the glucose and oxygen supply. Cancer Res. **46**, 3504–3512 (1986)
34. A. Friedman, A hierarchy of cancer models and their mathematical challenges. Discrete Contin. Dyn. Syst. B **4**, 147–159 (2004)
35. R.A. Gatenby, E.T. Gawlinski, A reaction-diffusion model for cancer invasion. Cancer Res. **56**, 5745–5753 (1996)
36. J.B. Gillen, E.A. Gaffney, N.K. Martin, P.K. Maini, A general reaction-diffusion model of acidity in cancer invasion. J. Math. Biol. (2013)
37. S. Goel, D.G. Duda, L. Xu, L.L. Munn, Y. Boucher, D. Fukumura, R.K. Jain, Normalization of the vasculature for treatment of cancer and other diseases. Physiol. Rev. **91**, 1071–1121 (2011)
38. P. Greenspan, Models for the growth of a solid tumour by diffusion. Stud. Appl. Math. **51**, 317–340 (1972)
39. P. Hahnfeldt, D. Panigrahy, J. Folkman, L. Hlatky, Tumor development under angiogenic signaling: a dynamical theory of tumor growth, treatment response, and postvascular dormancy. Cancer Res. **59**, 4770–4775 (1999)
40. M.A. Herrero, Reaction-diffusion systems: a mathematical biology approach, in *Cancer Modelling and Simulation*, ed. by L. Preziosi (Chapman and Hall, Boca Raton, 2003), pp. 367–420
41. T. Hillen, K.J. Painter, A user's guide to pde models for chemotaxis. J. Math. Biol. **58**, 183–217 (2009)
42. T. Hillen, H. Enderling, P. Hahnfeld, The tumor growth paradox and immune system-mediated selection for cancer stem cells. Bull. Math. Biol. **75**, 161–184 (2013)
43. P. Hinow, P. Gerlee, L.J. McCawley, V. Quaranta, M. Ciobanu, J.M. Graham, B.P. Ayati, J. Claridge, K.R. Swanson, M. Loveless, A.R.A. Anderson, A spatial model of tumor-host interaction: application of chemotherapy. Math. Biosci. Eng. **6**, 521–546 (2009)
44. D.G. Hirst, J. Denekamp, Tumour cell proliferation in relation to the vasculature. Cell Tissue Kinet. **12**, 31–42 (1979)
45. A. Iordan, A. Duperray, C. Verdier, A fractal approach to the rheology of concentrated cell suspensions. Phys. Rev. E **77**, 011911 (2008)
46. R.K. Jain, Normalizing tumor vasculature with anti-angiogenic therapy: a new paradigm for combination therapy. Nat. Med. **7**, 987–989 (2001)
47. H.V. Jain, A. Friedman, Modeling prostate cancer response to continuous versus intermittent androgen ablation therapy. Discrete Contin. Dyn. Syst. B **18**, 945–967 (2013)
48. K.A. Landman, C.P. Please, Tumour dynamics and necrosis: surface tension and stability. IMA J. Math. Appl. Med. Biol. **18**, 131–158 (2001)
49. U. Ledzewicz, M. Naghnaeian, H. Schättler, Optimal response to chemotherapy for a mathematical model of tumor-immune dynamics. J. Math. Biol. **64**, 557–77 (2012)
50. H.A. Levine, B.D. Sleeman, M. Nilsen-Hamilton, Mathematical modeling of the onset of capillary formation initiating angiogenesis. J. Math. Biol. **42**, 195–238 (2001)
51. J.S. Lowengrub, H.B. Frieboes, F. Jin, Y.L. Chuang, X. Li, P. Macklin, S.M. Wise, V. Cristini, Nonlinear modelling of cancer: bridging the gap between cells and tumours. Nonlinearity **23**, 1–91 (2010)

52. J.V. Moore, H.A. Hopkins, W.B. Looney, Dynamic histology of a rat hepatoma and the response to 5-fluorouracil. Cell Tissue Kinet. **13**, 53–63 (1980)
53. J.V. Moore, P.S. Hasleton, C.H. Buckley, Tumour cords in 52 human bronchial and cervical squamous cell carcinomas: inferences for their cellular kinetics and radiobiology. Br. J. Cancer **51**, 407–413 (1985)
54. M. Neeman, K.A. Jarrett, L.O. Sillerud, J.P. Freyer, Self-diffusion of water in multicellular spheroids measured by magnetic resonance microimaging. Cancer Res. **51**, 4072–4079 (1991)
55. P. Panorchan, M.S. Thompson, K.J. Davis, Y. Tseng, K. Konstantopoulos, D. Wirtz, Single-molecule analysis of cadherin-mediated cell–cell adhesion. J. Cell Sci. **119**, 66–74 (2006)
56. V.M. Perez-Garcia, G.F. Calvo, J. Belmonte-Beitia, D. Diego, L. Perez-Romasanta, Bright solitary waves in malignant gliomas. Phys. Rev. E **84**, 1–6 (2011)
57. L. Preziosi, G. Vitale, A multiphase model of tumor and tissue growth including cell adhesion and plastic reorganization. Math. Mod. Meth. Appl. Sci. **21**, 1901–1932 (2011)
58. K.R. Rajagopal, L. Tao, *Mechanics of Mixtures* (World Scientific, Singapore, 1995)
59. D. Ribatti, A. Vacca, M. Presta, The discovery of angiogenic factors: a historical review. General Pharmacol. **35**, 227–231 (2002)
60. J.M. Roda, L.A. Summer, R. Evans, G.S. Philips, C.B. Marsh, T.D. Eubank, Hypoxia-inducible factor-2α regulates GM-CSF-derived soluble vascular endothelial growth factor receptor 1 production from macrophages and inhibits tumor growth and angiogenesis. J. Immunol. **187**, 1970–1976 (2011)
61. J.M. Roda, Y. Wang, L. Sumner, G. Phillips, T.D. Eubank, C. Marsh, Stabilization of HIF-2α induces SVEGFR-1 production from Tumor-associated macrophages and enhances the Anti-tumor effects of GM-CSF in murine melanoma model. J. Immunol. **189**, 3168–3177 (2012)
62. A. Stephanou, S.R. McDougall, A.R.A. Anderson, M.A.J. Chaplain, Mathematical modelling of flow in 2d and 3d vascular networks: applications to anti-angiogenic and chemotherapeutic drug strategies. Math. Comput. Model. **41**, 1137–1156 (2005)
63. K.R. Swanson, C. Bridge, J.D. Murray, E.C. Alvord Jr., Virtual and real brain tumors: using mathematical modeling to quantify glioma growth and invasion. J. Neurol. Sci. **216**, 1–10 (2003)
64. K.R. Swanson, R. Rockne, J. Claridge, M.A. Chaplain, E.C. Alvord Jr., A.R.A. Anderson, Quantifying the role of angiogenesis in malignant progression of gliomas: In silico modeling integrates imaging and histology. Cancer Res. **71**, 7366–7375 (2011)
65. I.F. Tannock, The relation between cell proliferation and the vascular system in a transplanted mouse mammary tumour. Br. J. Cancer **22**, 258–273 (1968)
66. Y. Yang, L. Xing, Optimization of radiotherapy dose-time fractionation with consideration of tumor specific biology. Med. Phys. **32**, 3666–3677 (2005)

http://www.springer.com/978-1-4939-0457-0

Mathematical Oncology 2013
d'Onofrio, A.; Gandolfi, A. (Eds.)
2014, X, 334 p. 96 illus., 78 illus. in color., Hardcover
ISBN: 978-1-4939-0457-0
A product of Birkhäuser Basel